

PseudoTouch: Efficiently Imaging the Surface Feel of Objects for Robotic Manipulation.

Adrian Röfer*, Nick Heppert*, Abdallah Ayad, Eugenio Chisari, Abhinav Valada

Abstract—Humans seemingly incorporate potential touch signals in their perception. Our goal is to equip robots with a similar capability, which we term PseudoTouch. PseudoTouch aims to predict the expected touch signal based on a visual patch representing the touched area. We frame this problem as the task of learning a low-dimensional visual-tactile embedding, wherein we encode a depth patch from which we decode the tactile signal. To accomplish this task, we employ ReSkin, an inexpensive and replaceable magnetic-based tactile sensor. Using ReSkin, we collect and train PseudoTouch on a dataset comprising aligned tactile and visual data pairs obtained through random touching of eight basic geometric shapes. We demonstrate the efficacy of PseudoTouch through its application to two downstream tasks: object recognition and grasp stability prediction. In the object recognition task, we evaluate the learned embedding’s performance on a set of five basic geometric shapes and five household objects. Using PseudoTouch, we achieve an object recognition accuracy 84% after just ten touches, surpassing a proprioception baseline. For the grasp stability task, we use ACRONYM labels to train and evaluate a grasp success predictor using PseudoTouch’s predictions derived from virtual depth information. Our approach yields an impressive 32% absolute improvement in accuracy compared to the baseline relying on partial point cloud data. We make the data, code, and trained models publicly available at <http://pseudotouch.cs.uni-freiburg.de>.

I. INTRODUCTION

Successful dexterous object manipulation requires the ability to identify an object and track its state throughout the task. Robust vision-based methods for object detection [1], pose estimation [2], and tracking [3] have become ubiquitous in robotics. However, vision is an unreliable modality: the view of the object can be partially or fully occluded during the motion, or the space from which the object should be grasped can be completely unobservable. Moreover, the visual resolution can be simply insufficient for tracking a small object. Humans, on the other hand, are very capable of manipulating objects under heavy occlusion or total visual unobservability using their strong proprioceptive and tactile senses. Both senses are complementary to the visual sense, allowing a transition between the two: we can find a pen in a backpack or thread a screw into a hole without looking.

Existing works have used tactile embeddings for in-hand object pose estimation [4], [5], object recognition [6], and for improving robotic grasping [7]. However, the aforementioned works rely on tactile perception through an optical sensing systems, which have the disadvantages of high cost and

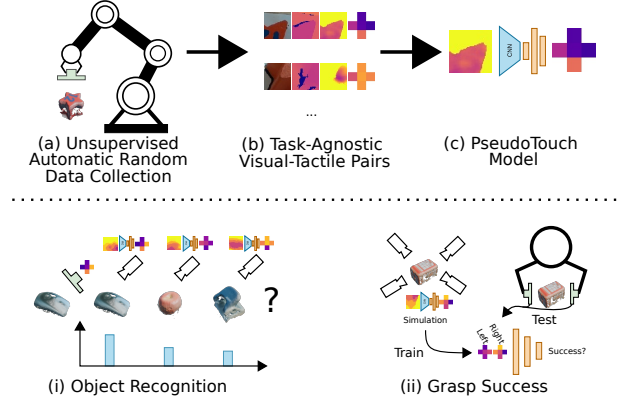


Fig. 1: Overview of PseudoTouch which infers the tactile signal given a visual input image. We use an unsupervised automatic data collection (a) to generate a dataset of task-agnostic visual-tactile pairs (b) used for training such an aforementioned model (c). We demonstrate the model’s utility in two downstream tasks. First, for object recognition (i) in which we compare PseudoTouch’s generated touch readings of potential objects to actually measured readings. Second, we use PseudoTouch to automatically enhance grasp labels with touch readings in a grasp stability prediction task (ii).

a bulky form factor. Furthermore, the high dimensionality of the optical sensing scheme requires a large number of training samples. We believe both of these aspects can be detrimental to the wide adoption of touch as a common robotic sensing modality. Bhirangi *et al.* [8] proposed a low-cost tactile sensor in a flat and optionally flexible form factor. Although the design is promising, it is so far largely unstudied. Different from its optical counterparts, ReSkin measures the magnetic field created by a magnetized gel pad placed on the sensor’s underside as five 3D field vectors. Contact with the pad deforms it and its field. This design presents two challenges: first, it is challenging to simulate, and second, the low dimensionality of the reading limits the information that can be extracted from it. In this work, we investigate using the ReSkin sensor as a platform to learn a visual-tactile embedding, which allows us to infer tactile readings from depth images. We evaluate the performance of the method on two downstream tasks: object recognition and grasp stability prediction. We show that despite the low dimensional sensor readings, our method is able to achieve competitive results on these tasks. We additionally conduct a user study to compare our model to a human touch baseline, whose result highlights the difficulty of the tasks and the effectiveness of our approach.

The main contributions are as follows:

- A model architecture for successfully inferring tactile readings from depth images.

* These authors contributed equally.

Department of Computer Science, University of Freiburg, Germany. This work was funded by the Carl Zeiss Foundation with the ReScaLe project and the BrainLinks-BrainTools center of the University of Freiburg.

- A data-collection and training setup that allows training our model using a small amount of data.
- Two demonstrator applications were used to evaluate the utility of our learned model, an object recognition task and a grasp quality prediction task.
- Code, trained models, and data are made publicly available at <http://pseudotouch.cs.uni-freiburg.de>.

II. RELATED WORK

We first highlight recent developments of tactile sensors with a specific focus on comparing low-resolution sensors that are inexpensive to high-resolution sensors that are more expensive. Second, we provide insights into previous visual-tactile cross-modality learning approaches. Lastly, we briefly introduce current approaches for our proposed downstream tasks and how PseudoTouch can enhance these approaches.

A. Tactile Sensors

Tactile sensing has long been of interest in robotic manipulation and various approaches have been used to build tactile sensors for robots. In recent years, vision-based sensors have become a very prominent technique in tactile sensing for robotics. Sensors such as GelSight [9], DIGIT [10], and DigiTac [11], consist of an elastomer observed by a camera. Due to tracking markers on the elastomer, or multi-colored light sources in the sensor, deformations caused by contact can be observed by the camera. This visual paradigm delivers very high-resolution impressions of the touched surface and can be simulated easily using standard computer graphic rendering techniques [12]. Especially the simulatability makes these sensors prime candidates for reinforcement learning approaches. However, these sensors are expensive, with Digit being the cheapest at 300\$ per sensor. In addition, they require space between the optical sensor and the elastomer, leading to a bulky form factor. Lastly, the need for optical observation prevents these approaches from scaling beyond small, even surfaces.

Alternatively, there are numerous approaches that use low-resolution sensors to measure quantities that can be affected by physical force. Early works, such as [13], use liquid-filled elastomers that change their electrical impedance under pressure and measure this impedance using multiple small sensors. More modern designs use a combination of pressure and proximity sensing [14] to measure contact force and location at high frequencies. Tactile sensors based on magnetism always consist of magnetometers and a magnetic field that is affected by contact. In [15], the authors suspend a single small magnet in an elastomer dome above four magnetometers, which allows to achieve robustness against stray magnetic fields and to be able to measure contact force magnitude and direction. While this design is very affordable and robust, it cannot be used to distinguish the shapes of stationary contacts. ReSkin [16] and [17] both use an array of magnetometers to measure the magnetic field of a magnetized elastomer placed above them. Using neural networks, both approaches are able to learn a prediction of the contact point and force on the elastomer. In [16], the authors also demonstrate that their design can be printed onto

a flexible PCB, which allows their ReSkin sensor to act as a skin that can be attached to curved and soft surfaces.

B. Visual-Tactile Embeddings

Combining different modalities through a common embedding has been widely researched [18], [19]. Specifically, the combination of visual and tactile modalities has been used for reconstructing 3D shapes [20], [21]. Here, typically the choice for fusing both modalities is at the point cloud level [22]. While [23] still uses point clouds as their fusion representation, they investigate how to define descriptors for both the visual point clouds and tactile point clouds. In a follow-up work [24], the authors investigate how to minimize a distribution shift between both descriptors. [25] fuses both modalities in a common embedding space trained end-to-end and used for a downstream robotic manipulation task, whereas [26] learns an implicit representation of shape and tactile through a neural radiance field [27], which first renders color and depth images given a camera pose and then generate the corresponding touch reading. Closest to our work is [28], [29], which predicts the touch signal from an RGB image and vice versa. [30] go even one step further and include audio and text. Opposed to other works, the ReSkin sensor we use is low dimensional and cannot be easily transformed into a local point cloud, making previous object-centric representations unsuitable. Thus, we learn a cross-modal embedding focused on a small local patch which can be for instance, as demonstrated in our object recognition task, to build an object-centric representation again.

C. Down Stream Tasks

There have been several uses of learned tactile models in robotics. For a common robotics task, [4] performs in-hand object recognition and pose estimation by training an embedding model on simulated data using CAD models. During inference, they infer the correct object pose distribution by matching their embedding of the sensor data with the embeddings of their simulated data. Following up on their proposal of the ReSkin sensor, Bhirangi *et al.* [16] use ReSkin sensors to build a low-cost robotic hand with tactile sensing. Aside from demonstrating the physical capabilities of their prototype, they also train classifiers for material, texture, and softness identification. They generate data using a simple motor-babbling policy and feed this data through an LSTM followed by multiple linear layers with ReLU activations. They achieve 65% accuracy in these tasks when deploying their models on unseen objects. Most closely related to our downstream task of object recognition, [6] addresses object recognition using tactile sensing. Using a sensor that can only measure a contact point and the surface normal, they train an exploration policy and a discriminator to propose new sample points and to predict the object class. Both of these modules work off of a point cloud encoder which encodes the already sampled contact points and their normals. They show very high accuracy in object identification while requiring significantly fewer sample points than their baselines. Also similar to our downstream task of object recognition, [31] study the problem of learning object recognition using an array

of pressure sensors. They focus on building an incremental tactile model of objects by having the robot explore them and store the information in a 3d representation. This differs from our downstream task in that we are proposing a pretrained model that can predict these readings outright.

Grasp Stability Prediction: Previously [7], [32] showed that predicting grasp stability with tactile signals outperforms a pure visual baseline. While [7] were able to collect a large dataset in simulation as they used a simulatable vision-based tactile sensor, [32] collected a large real-world dataset. By using PseudoTouch to generate tactile readings for simulated visual patches, we can use pre-annotated grasp stability datasets to generate a dataset, avoiding the need to either simulate a touch sensor or collect extensive real-world grasp labels with a tactile sensor.

III. TECHNICAL APPROACH

We first detail our PseudoTouch approach and then describe how we exploit it for the two downstream tasks.

A. PseudoTouch-Model

Our proposed model is a function $PT : z_d \Rightarrow \tilde{\tau}$, which takes a depth image $z_d \in \mathbb{R}^{17 \times 17}$ of the object surface as input, and predicts the tactile reading that would be emitted touching the surface $\tilde{\tau} \in \mathbb{R}^{15}$. We implement this function as a neural network, consisting of a light-weight convolutional encoder, followed by a flattening average pooling, the output of which is fed through a single layer MLP before predicting the tactile reading $\tilde{\tau}$. We choose a very low-capacity model to prevent overfitting on our small dataset and due to the large size imbalance between the input and output of our network.

To evaluate the model architecture, we propose a custom *order accuracy* metric. This metric captures ReSkin magnetometers activation similarity between the ground truth touch signal and the inferred touch signal. We compose it using two components. The first component is the sorted position sub-metric. It scores one point for each magnetometer measurement, in the inferred signal, that is placed in the same order as the corresponding one in the ground truth touch signal, after taking the norm and sorting the magnetometer values in both signals as

$$\|\tilde{\tau}_j\|_2 = \sqrt{\sum_{i=x,y,z} \tau_{ji}^2}, j \in \{1, \dots, 5\}, \quad (1)$$

where $\tilde{\tau} \in \mathbb{R}^{5 \times 3}$ is the spatially distributed touch signal, and $\hat{\tau} = (\hat{\tau}_1, \hat{\tau}_2, \hat{\tau}_3, \hat{\tau}_4, \hat{\tau}_5)$ is the sorted sequence of the normed values. For simplicity, we will use $\tau \in \mathbb{R}^5$ as the normed unsorted signal from now on in this section.

The second component is the pairwise order sub-metric. It compares each magnetometer measurement with its four counterparts in a signal, without sorting their values, to determine the relation between each pair, thus we get $\binom{5}{2}$ relations. For every similar relation among the inferred signal and the ground truth signal, we increment the scored points by one. Aggregating the two components, we divide each sub-metric scored points by the total number of possible

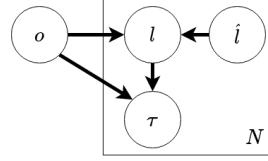


Fig. 2: Object Recognition Model. o is an object hypothesis, l is the location where the actual touch was recorded, \tilde{l} is the location where we intended to touch and τ is the actual result of our touch. N is the number of all touches performed.

points for it and then take the average among them. First, we formally define our sorted position metric.

Let $\hat{\tau}$ and $\hat{\tau}_{\text{gt}}$ denote the sorted lists of the inferred and ground truth normed signals, respectively. The metric O_p is then given by

$$O_p = \sum_{k=1}^5 \llbracket \text{index}(\hat{\tau}, \hat{\tau})_k = \text{index}(\tau_{\text{gt}}, \hat{\tau}_{\text{gt}})_k \rrbracket, \quad (2)$$

where $\llbracket \bullet \rrbracket$ is the Iverson bracket and $\text{index}(\tau, \hat{\tau})_k$ represents the index of the normed magnetometer value in the sorted list $\hat{\tau}$, such that this value is in the k^{th} position in τ .

Second, we define our pairwise order metric O_r as

$$O_r = \sum_{i=1}^5 \sum_{j=i+1}^5 \llbracket \llbracket \hat{\tau}_i > \hat{\tau}_j \rrbracket = \llbracket \tau_{\text{gt},i} > \tau_{\text{gt},j} \rrbracket \rrbracket. \quad (3)$$

The order accuracy O is then defined as the average between the pairwise order sub-metric O_r and the sorted position sub-metric O_p , calculated as

$$O = \frac{1}{2} \left(\frac{O_p}{5} + \frac{O_r}{\binom{5}{2}} \right). \quad (4)$$

B. Online Object Recognition

In the first downstream task, we use PseudoTouch to recognize objects from a given set of candidate objects. To this end, we subsequently perform N touches and update our current object hypothesis based on the touch result through a Markov model.

Algorithmic Outline: We assume we are given a set of objects O with known 3D representation (e.g. meshes/surfaces), denoted by \mathcal{P}_o for object o . For our maximum number of touches N , we calculate the current object likelihood given the current observations consisting of previous touch locations $L = \{l_1, \dots, l_i\}$ and readings $T = \{\tau_1, \dots, \tau_i\}$ and sample from that distribution to get an object hypothesis \tilde{o} on which we will randomly sample a location \tilde{l} . To perform the touch at the specified location, we move the robot there along the normal until the measured force exceeds a threshold. We then record the position of the end-effector and touch signal and feed it into the pool of observations.

Markov Formulation: We formulate the object recognition task as a classical directed graphical model (refer to Fig. 2).

The full probability for a single touch is given through

$$p(o, \tilde{l}, l, \tau) = p(o) p(\tau | l, o) p(l | o) p(\tilde{l} | \tilde{l}) p(\tilde{l}) \quad (5)$$

assuming conditional independence between the object o and \tilde{l} . In the following, we define each probability. Initially, we assume a uniform prior for each object o

$$p(o) = \frac{1}{|O|} \quad (6)$$

over the set of all objects O . We introduce probabilities for touch and proprioception observations.

Given the results of a touch τ , we formulate the touch likelihood for each object o as

$$p(\tau | o, l) = \exp(-\|\tilde{\tau}_o - \tau\|), \quad (7)$$

where $\tilde{\tau} = PT(\tilde{z}_d(o, l))$ is the predicted hypothesized touch $\tilde{\tau}_o$ for an object o at location l_i based on the simulated depth patch $\tilde{z}_d(o, l)$.

Similarly, we define the proprioception likelihood as

$$p(l | o) = \exp(-\|\min(l, \mathcal{P}_o)\|), \quad (8)$$

where $\min(l, \mathcal{P}) = \min_{p \in \mathcal{P}} \|l - p\|$ is the minimum distance from the location l to a point p on the objects surface \mathcal{P} .

The probability of the actual recorded touch location l and the desired touch location \tilde{l} can be assumed constant with α

$$p(l | \tilde{l}) = \alpha \quad (9)$$

as the actual touch location is not directly dependent on the desired location. Similarly, we simplify the probability of the desired touch location \tilde{l}

$$p(\tilde{l}) = \alpha \quad (10)$$

to be constant for some value α .

After performing N touches we will have a set of proprioceptive and touch reading tuples, each given as (τ_n, l_n) for the n -th touch as well as desired touch location (\tilde{l}_n) . Assuming we performed N touches in total, we formulate the full joint probability of an object o as

$$p(o, (\tau_1, l_1), \dots, (\tau_N, l_N), \tilde{l}_1, \dots, \tilde{l}_N) = p(o) \prod_n p(\tau_n | l_n, o) p(l_n | o) \quad (11)$$

already leaving out $p(l_n | \tilde{l}_n)$ and $p(\tilde{l}_n)$ for clarity as they will be eventually eliminated in a normalization step. Further, the probability of an object o given the current observations is described by

$$p(o | (\tau_1, l_1), \dots, (\tau_N, l_N), \tilde{l}_1, \dots, \tilde{l}_N) = \frac{p(o, (\tau_1, l_1), \dots, (\tau_N, l_N), \tilde{l}_1, \dots, \tilde{l}_N)}{p((\tau_1, l_1), \dots, (\tau_N, l_N), \tilde{l}_1, \dots, \tilde{l}_N)}, \quad (12)$$

where the denominator is given through marginalizing Eq. (11) over all $\tilde{o} \in O$.

In each step we then pick the object

$$o = \arg \max_{\tilde{o}} p(o | (\tau_1, l_1), \dots, (\tau_N, l_N), \tilde{l}_1, \dots, \tilde{l}_N) \quad (13)$$

that best explains the current observations.

C. Grasp Stability Prediction

In the second downstream task, we use PseudoTouch to predict the grasp success on an object. We setup a neural network $GQ_\tau(\tau_l, \tau_r) = s$ that uses the tactile readings from the left τ_l and the right finger τ_r ReSkin as input and infers a binary score $s \in [0, 1]$ indicating the potential success of the grasp. To train such a network, the straightforward but time-intensive approach would be to collect a training dataset by executing many grasps on real objects recording the touch signal just before the grasp happens, and labeling them with the observed grasp outcome [32].

In contrast, we leverage our proposed PseudoTouch and recent advancements in large-scale simulations to generate a training, validation, and test set for the aforementioned grasp stability predictor. Given an object from the ACRONYM dataset, we set up a virtual renderer in which we use two orthographic virtual cameras at the fingertips of the gripper at the grasp $g \in SE(3)$ to render mask patches for the left $m_l \in \mathbb{R}^{D \times D}$ and right finger $m_r \in \mathbb{R}^{D \times D}$. We then use PseudoTouch (trained on random touches) to infer a virtual tactile signal. Hence, we generate a large-scale dataset to train and test the grasp quality predictor GQ_τ without the need to execute and annotate real grasps.

IV. DATA COLLECTION

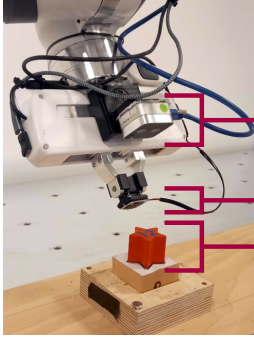
To train and evaluate our model, we collect a dataset consisting of tactile readings $\tau \in \mathbb{R}^{15}$ and the depth image $z_d \in \mathbb{R}^{17 \times 17}$ of the corresponding 17 mm \times 17 mm area that was touched by the sensor. The collection process is semi-automated as we detail in the following section.

A. Robotic Setup

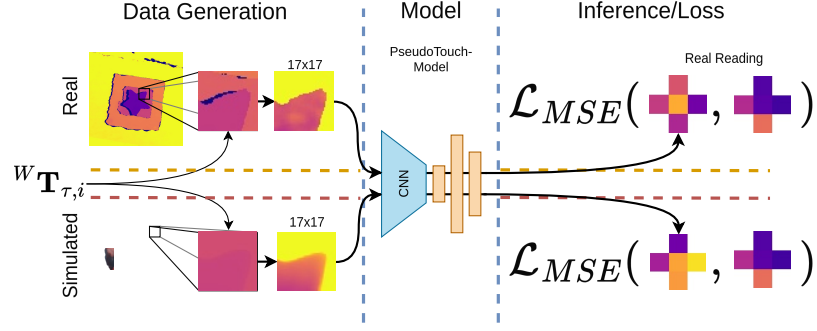
We use a table-mounted Franka Emika robot with a wrist-mounted D405 Realsense RGBD camera and a 3D-printed *finger* holding the ReSkin sensor at its end. The objects are fixed on wooden bases which sit firmly in a wooden socket mounted to the table. The full setup is displayed in Fig. 3.

Our data collection procedure consists of 6 steps:

- 1) Starting with a robot with correct hand-camera calibration, we use Franka's hand-guiding feature to guide the camera around an object and collect 10 RGBD images. We convert these into point clouds which we prune for all all points that are outside of the object's volume. We integrate the remaining points into a volume [33], from which we finally extract a surface mesh m .
- 2) We sample candidate points $C_m = \{(\mathbf{p}_1, \mathbf{n}_1), \dots, (\mathbf{p}_I, \mathbf{n}_I)\}$ from the mesh m by uniformly sampling from it vertices \mathbf{p}_i and their corresponding normals \mathbf{n}_i . We reject samples if the normal's angle to the table is flatter than 33° , or we find that the approach corridor along the normal is obstructed.
- 3) To observe the target zone before touching, we define an IK-problem that places the wrist camera along the normal \mathbf{n}_i , 12 cm away from \mathbf{p}_i with the camera's optical axis facing along the normal towards the point. We use the same formulation for defining the *pre-touch* pose of the end-effector, where we recycle the solution for the



(a) Robotic setup for data collection.



(b) Flow of data from depth image to prediction.

Fig. 3: (a): Overview of physical robot setup for data collection. The ReSkin sensor is attached as a fingertip to the gripper of the robot. Using the Realsense D405 camera, we capture an image before touching the object. The object is attached to a wooden anchor which is mounted to the table for repeatability. (b): Illustration of data processing and inference. From a real depth image, we crop the section that the robot touched using the recorded end-effector pose ${}^W\mathbf{T}_{\tau,i}$. To mitigate the gap between real and simulated data, we use the same pose and a mesh of the object to render a simulated sample. We normalize both depth patches and pass them through our PseudoTouch model. Finally, we minimize the L1-loss deviation from the actual sensor reading.

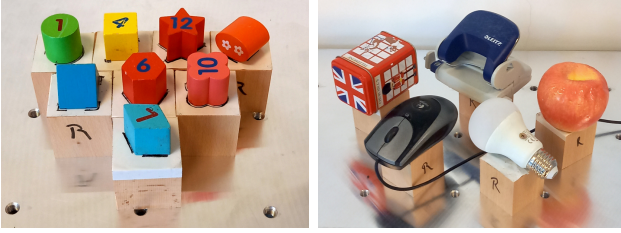


Fig. 4: Objects used for training and validation of PseudoTouch. Left: Primitive shape objects used for training. Right: Everyday objects used for object recognition experiments for validation. In clock-wise order starting at the 12 o'clock position: *puncher*, *apple*, *bulb*, *pc mouse*, *tin box*.

camera pose. Because of the small size of the sensor, we require very precise solutions to ensure minimal deviation from the target. We use [34] to obtain solutions and reject them if they deviate by more than 5 mm or 5°.

- 4) Once the IK-solutions were obtained successfully, we move the robot to the first one, take an RGBD observation z_i and the camera pose ${}^W\mathbf{T}_{c,i}$.
- 5) Subsequently, we move the robot to its pre-touch pose. We obtain an ambient reading $\hat{\tau}_i$ by averaging 50 readings collected in this position. We move on to touching the object by moving the end-effector towards \mathbf{p}_i along \mathbf{n}_i at 1.5 cm s^{-1} until we read the relevant deviation of the sensor measurements from the ambient reading. We collect an averaged reading $\hat{\tau}'_i$ of 40 samples which we use to calculate the dataset item $\tau_i = \hat{\tau}'_i - \hat{\tau}_i$. Along with the tactile measurement, we also record the pose ${}^W\mathbf{T}_{\tau,i} \in SE3$ in which the end-effector made contact with the object.
- 6) The patch is extracted by projecting the sensor's corners into the z_i using ${}^c\mathbf{T}_{\tau,i} = {}^W\mathbf{T}_{c,i}^{-1} {}^W\mathbf{T}_{\tau,i}$. We warp the enclosed depth image into a square and resize it to its target resolution obtaining our raw depth patch $\hat{z}_{d,i}$.

B. Objects and Dataset Extension

We collect data from 8 primitive objects from a shape-sorting toy. As shown in Fig. 4, these objects comprise different geometric features such as edges of different curvatures and points of different sharpness. We train our model only on

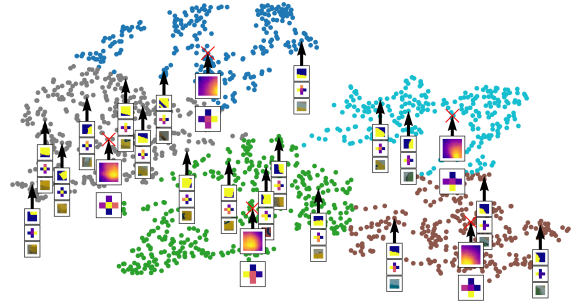


Fig. 5: t-SNE plot of our data distribution. Five-means clustering of our tactile data points with the associated depth images, tactile visualizations, and RGB images for example points. The means of the clusters are projected and highlighted in red with associated mean depth images and mean tactile visualizations. The means show the spatial correspondence between the depth images and the tactile signals visualizations.

data gathered from these objects. We collect 1600 samples from these objects. Fig. 5 presents the distribution of the data. We first observe qualitatively that our collected touch signals are distributed over the area of ReSkin sensor. Second, we observe the spatial structure similarity between our touch signals and their depth counterparts, which indicates that learning one modality from the other is possible. As shown in Fig. 3, we observe a large gap between the real depth patches and their simulated equivalent. This presents a challenge, as our downstream tasks are based on simulated depth data, the real and simulated data need to be very closely aligned. Instead of integrating a more realistic rendering model, we choose to train the model to close the gap between our real and simulated observations. We do so by adding a second sample (τ_i, \hat{z}_d) for each sample (τ_i, z_d) in our dataset, with \hat{z}_d being a virtual depth patch obtained from a simulation environment.

V. EXPERIMENTS

We perform three experiments. The first experiment in Sec. V-A demonstrates that meaningful features can be extracted from the ReSkin sensor by performing a classification

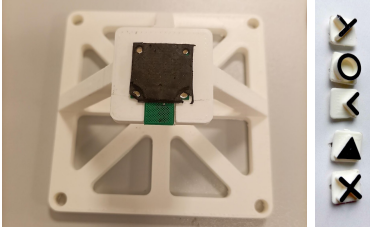


Fig. 6: Shape classification experiment setup. Left: The ReSkin sensor is mounted atop a static fixture such that the robot can access it from the top. Right: We use differently shaped *stamps* to indent the gel pad in different locations. From top to bottom the shapes are: *T*, *circle*, *angle*, *triangle*, *cross*. All stamps have a maximum extent of 10 mm and a profile depth of 3.5 mm.

	Primitives Objects			Everyday Objects		
	P	T	P+T	P	T	P+T
<i>Human Baseline</i>	34%	60%	71%	51%	77%	86%
PseudoTouch ($N = 5$)	12%	42%	42%	60%	84%	64%
PseudoTouch ($N = 150$)	24%	47%	47%	53%	62%	60%

TABLE I: Results of the object recognition experiment. We compare the baselines on two object sets (primitives and everyday) with 3 different input modalities: proprioception (P), touch (T), and both together (P+T). Our proposed PseudoTouch is evaluated with ($N = 5$) importance sampling as well as without ($N = 150$). We also add the human baseline from our user study to put the results in perspective.

task on multi-touch contacts. The second experiment in Sec. V-B utilizes PseudoTouch as described in Sec. III-B to perform object recognition. Lastly, the third experiment in Sec. V-C performs the grasp stability prediction outlined in Sec. III-C.

A. Shape Classification

At the onset, we hypothesized that it would be very challenging to recognize complex touches with the ReSkin sensor. In the original work [8], Bhirangi *et al.* demonstrate that it is feasible to identify exact touch locations and interaction forces. However, it is not clear that one can also distinguish between different larger contact areas and different shapes of these areas. To verify that the sensor can indeed be used for this purpose, we performed a preliminary experiment where we fixed the ReSkin sensor in a location and then indented its surface in regular intervals with differently shaped stamps. This setup and the stamps are shown in Fig. 6.

We indent the sensor with each stamp multiple times on a 2D grid and use the robot’s proprioceptive force sensing to decide when to record a touch sample. Using this setup, we collect a dataset of 1280 datapoints and split them into chunks of 70% for training, 10% for validation, and 20% to report test accuracy. We train single-layer MLP with a hidden layer of size 200 and a 5-class classification head using cross-entropy loss optimized with ADAM with a learning rate of 10^{-3} . The best performing model according to our validation set achieves an accuracy of 92% for correctly classifying the shape on the left-out test set. Thus, we conclude that the sensor data can be used to distinguish between different contact shapes.

B. Object Recognition

For the first downstream task, we evaluate the performance of PseudoTouch for the object recognition task. Akin to reaching into a backpack for a pen, in this task, the agent needs to identify the correct object out of a given candidate set. We assume that the agent has detailed 3D models such as CAD models or 3D scans of the candidate objects to predict the sensor measurements that should have been observed when touching an object. We use the probabilistic inference formulation from Sec. III-B and compare the performance of touch, proprioception (i.e. contact location), and their combination. We set the expected variance $\sigma = 8.6$ for touch, and $\sigma = 0.0088$ for proprioception. We extract these values from the dataset’s validation set. The touch variance is the measured variance on the trained model predictions whereas the proprioception variance is calculated from the collected dataset by measuring the mean distance between the sampled and actual touch location.

Experimental Setup: We perform the experiment on two sets of objects: the primitives from which we also collected our training data and a set of real everyday objects. Both these object sets are shown in Fig. 4. We only use a subset of five objects of the primitives to make the experiments more comparable. We pick *square* (4), *hexagon* (6), *cylinder* (1), *star* (12), and *flower* (10) (the number in parentheses references the number printed on the object for easier identification). As we do not focus on pose estimation, we fix the objects to wooden bases so that they do not move nor turn when the robot interacts with them. The 3D scans we take of the objects reflect this setup. Each experiment consists of an object being touched 10 times in locations sampled according to our approach described in Sec. III-B. We repeat each experiment 5 times for each object and report the success rate of the three different conditions in correctly identifying the object. Additionally, we perform an ablation study with all $10 \times 5 \times 3 \times 5 = 750$ samples we obtain for each object set where we ignore the informed object hypothesis procedure and randomly sample from the collection of all recorded samples according to the ground truth object ($N = 150$). As a result, all modalities draw samples from the same distribution and thus, are more comparable.

User Study: Furthermore, we conducted a user study with five participants unfamiliar with this work and with the same object sets to evaluate the performance of the human touch sense on the object recognition task. Each participant is shown a picture of the object sets during the evaluation. We sample an object randomly, let the person touch it 10 times with one finger without looking at it, and then record whether they are able to recognize it. We repeat the process for each object set and each modality 7 times, and average the results.

Results: We present the results in Tab. I. We find both methods to work well for the everyday object set, especially with the informed object sampling with touch performing 20% better than proprioception. This trend is also present for the primitive recognition task, although at a much lower performance for both methods. This is expected, as these objects are much more similar to one another in their extent and surface

features. As we discard the informed object sampling, the gap between the approaches narrows significantly. In the case of the primitives, both methods improve, with proprioception benefiting the most. In the everyday objects, the performance of both marginally diminishes. This signifies that informed sampling is detrimental to the primitive recognition task, as it can lead to an incorrect hypothesis which it then reinforces due to the similarity of the objects. Conversely, in the real object task, it helps due to the dissimilarity of the objects. Interestingly, we obtain inferior performance for the combination of both modalities. Upon analyzing the failures, we find that our chosen variance for proprioception is too narrow, leading to an aggressive diminishing of the estimate when the measured end-effector position deviates too much from the prediction. Increasing the variance improves joint prediction, but does not change the relative performance of the methods, which is why we choose not to ablate this change in detail here. Finally, we note how the PseudoTouch and the human baseline results follow similar trends, validating our findings. While the human baseline scores on average higher success, the difference is moderate, highlighting the efficacy of our learned system. In conclusion, we find that our PseudoTouch model does transfer to predicting touch signals outside of its original training distribution, achieving 84% accuracy on the tactile object recognition task with everyday household objects.

C. Grasp Quality Prediction

For the second downstream task, we show that PseudoTouch can be leveraged to generate grasp labels for training a tactile grasp success predictor. We compare such a predictor against a baseline which uses point clouds as input.

Simulation: As described in Sec. III-C, we first generate a large-scale dataset using PyBullet as our renderer. We use objects from the ShapeNetSem object set [35] and pre-annotated grasps from ACRONYM [36] which has annotated grasps for more than 8800 objects (the same object instance with a different scale is considered a different object). For each of the objects, we randomly sample five successful and five unsuccessful grasps and record the depth patches $d_l, d_r \in \mathbb{R}^{48 \times 48}$ for each finger using a virtual orthographic camera. We convert the depth patches to mask patches m_l, m_r similar to the real data. For each object, we randomly sample ten random camera poses and extract object point clouds. We use the same set of grasps but throw away grasps that do not face the camera determined by the angle between the grasp direction and the camera normal. If the angle is above 85° , the grasp is considered invalid. During training, we randomly downsample the point cloud to 2048 points at each batch. Overall, due to some imperfect meshes in ShapeNetSem, we have roughly 8500 objects which we split into a train (70%), validation (10%), and test set (20%), giving us a total of 58770 data points for training the tactile network and 253508 data points to train the point cloud network.

Real World: To demonstrate that PseudoTouch easily transfers to the real world, we perform a real grasping experiment. As shown in Fig. 7, we replace the single ReSkin touch sensor

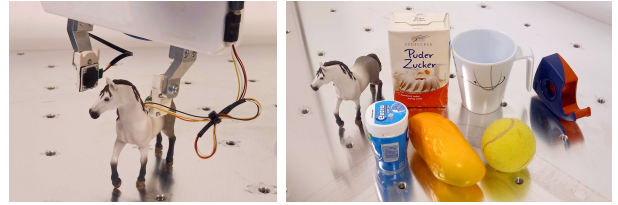


Fig. 7: **Left:** Setup for grasping with ReSkin sensors. We 3D-print two fingers for the sensors, which possess suitable bores for mounting the sensors and gel pads to them. The microcontrollers are attached to the gripper, and the wires are left floating loosely so they do not get strained by the movement of the fingers. **Right:** Overview of our objects used in our grasping validation. With the objects, we try to cover a range of different shapes and weights. *Back row:* Toy horse, pack of sugar, cup, tape dispenser. *Front row:* Gum can, mango, tennis ball.

Modality	Sim Acc. (\uparrow)	Real Acc. (\uparrow)
$GQ_{\mathcal{P}}$ (PC)	64%	47%
PseudoTouch (T) + $GQ_{\mathcal{P}}$ (PC)	73%	36%
PseudoTouch (T)	76%	79%

TABLE II: Results for grasp quality prediction using different modalities: Point Clouds (PC) from $GQ_{\mathcal{P}}$ and Tactile (T) from PseudoTouch. For each modality, we report the accuracy of the grasp success prediction.

on the robotic gripper with a ReSkin sensor mounted on each finger. To predict grasps, we use ContactGraspNet [37], an off-the-shelf grasping network. We place a single object on a table. After acquiring a suitable grasp, we move the robot towards it and slowly close the gripper until both of the ReSkin sensors measure a significant activation or the gripper is stalled. We then record the signal for both, attempt the grasp, and manually label it as successful or not. Overall, we recorded 76 grasps across 7 objects (refer to Fig. 7). To extract object point clouds as ContactGraspNet, we use [38] to detect the object mask which is then projected into 3D using the depth image and the camera’s intrinsic.

Baseline: Our baseline adapts [7], [32] and uses a learned neural network $GQ_{\mathcal{P}}$ that processes a partial point cloud. The point cloud is first processed with an XYZ-feature-aware PointNet++ backbone [39] before it is down-pooled and concatenated with the grasp $g \in SE(3)$ (expressed as $\mathbb{R}^{4 \times 4}$). These features are then given to two fully connected layers to infer the grasp success score s . We use the same renderer as described above but render point clouds of the object using an external camera.

Results: We show the results of our grasp quality predictor in Tab. II. We observe that the model solely trained on touch data outperforms both baseline models. This can be attributed to the fact that the point cloud simulation does not include realistic sensor noise which shows that using a low-dimensional sensor such as the ReSkin transfers more readily to a sim-to-real setup as opposed to higher-dimensional sensors such as cameras.

VI. CONCLUSION

In this work, we investigated the use of the novel ReSkin sensor for general robotic tasks. Unlike its vision-based counterparts, this sensor is attractive for its compact form factor and low cost. However, its low-dimensional readings raise the question of whether it can be used for tasks that

require more advanced tactile distinction. Towards this goal, we proposed PseudoTouch, a novel approach that infers expected tactile readings from small depth images of surfaces. We introduced a low-dimensional model architecture and a procedure for collecting data to train the model, including a data augmentation strategy. By pretraining the model on one set of objects and leveraging it for separate downstream tasks, we demonstrated that our model can transfer successfully outside of its object training distribution. We view our results as an encouraging step towards using inexpensive tactile sensors such as ReSkin more often in robotics. For future work, we see an opportunity for building the inverse of our approach: a model predicting depth images from tactile signals to obtain 3D object features. This would enable our approach to perform full tactile 3D reconstruction.

REFERENCES

- [1] C. Lang, A. Braun, and A. Valada, "Robust object detection using knowledge graph embeddings," in *DAGM German Conference on Pattern Recognition*, 2022, pp. 445–461.
- [2] E. Chisari, N. Heppert, T. Welschhold, W. Burgard, and A. Valada, "Centergrasp: Object-aware implicit representation learning for simultaneous shape reconstruction and 6-dof grasp estimation," *arXiv preprint arXiv:2312.08240*, 2023.
- [3] J. O. von Hartz, E. Chisari, T. Welschhold, W. Burgard, J. Boedecker, and A. Valada, "The treachery of images: Bayesian scene keypoints for deep policy learning in robotic manipulation," *IEEE Robotics and Automation Letters*, 2023.
- [4] M. Bauza, A. Bronars, and A. Rodriguez, "Tac2pose: Tactile object pose estimation from the first touch," *arXiv preprint arXiv:2204.11701*, 2022.
- [5] R. Buchanan, A. Röfer, J. Moura, A. Valada, and S. Vijayakumar, "Online estimation of articulated objects with factor graphs using vision and proprioceptive sensing," *arXiv preprint arXiv:2309.16343*, 2023.
- [6] J. Xu, H. Lin, S. Song, and M. Ciocarlie, "Tandem3d: Active tactile exploration for 3d object recognition," in *Proc. IEEE Int. Conf. on Rob. and Auto.*, 2023, pp. 10401–10407.
- [7] L. Chumbley, M. Gu, R. Newbury, J. Leitner, and A. Cosgun, "Integrating high-resolution tactile sensing into grasp stability prediction," in *Conference on Robots and Vision*, 2022, pp. 98–105.
- [8] R. Bhirangi, T. Hellebrekers, C. Majidi, and A. Gupta, "Reskin: versatile, replaceable, lasting tactile skins," in *Proc. Conf. on Rob. Learn.*, 2021.
- [9] W. Yuan, S. Dong, and E. H. Adelson, "Gelsight: High-resolution robot tactile sensors for estimating geometry and force," *IEEE Sensors*, vol. 17, no. 12, p. 2762, 2017.
- [10] M. Lambeta, P.-W. Chou, S. Tian, B. Yang, B. Maloon *et al.*, "Digit: A novel design for a low-cost compact high-resolution tactile sensor with application to in-hand manipulation," *IEEE Robotics and Automation Letters*, vol. 5, no. 3, pp. 3838–3845, 2020.
- [11] N. F. Lepora, Y. Lin, B. Money-Coomes, and J. Lloyd, "Digitac: A digit-tactile hybrid tactile sensor for comparing low-cost high-resolution robot touch," *IEEE Robotics and Automation Letters*, vol. 7, no. 4, pp. 9382–9388, 2022.
- [12] S. Wang, M. Lambeta, P.-W. Chou, and R. Calandra, "Tacto: A fast, flexible, and open-source simulator for high-resolution vision-based tactile sensors," *IEEE Robotics and Automation Letters*, vol. 7, no. 2, pp. 3930–3937, 2022.
- [13] N. Wettels, V. J. Santos, R. S. Johansson, and G. E. Loeb, "Biomimetic tactile sensor array," *Advanced Robotics*, vol. 22, no. 8, pp. 829–849, 2008.
- [14] A. SaLoutos, E. Stanger-Jones, M. Guo, H. Kim, and S. Kim, "Design of a multimodal fingertip sensor for dynamic manipulation," in *Proc. IEEE Int. Conf. on Rob. and Auto.*, 2023, pp. 8017–8024.
- [15] T. Le Signor, N. Dupré, and G. F. Close, "A gradiometric magnetic force sensor immune to stray magnetic fields for robotic hands and grippers," *IEEE Robotics and Automation Letters*, vol. 7, no. 2, pp. 3070–3076, 2022.
- [16] R. Bhirangi, A. DeFranco, J. Adkins, C. Majidi, A. Gupta, T. Hellebrekers, and V. Kumar, "All the feels: A dexterous hand with large area sensing," *arXiv preprint arXiv:2210.15658*, 2022.
- [17] Y. Yan, Z. Hu, Z. Yang, W. Yuan, C. Song, J. Pan, and Y. Shen, "Soft magnetic skin for super-resolution tactile sensing with force self-decoupling," *Sci. Robot.*, vol. 6, no. 51, p. eabc8801, 2021.
- [18] A. Younes, D. Honerkamp, T. Welschhold, and A. Valada, "Catch me if you hear me: Audio-visual navigation in complex unmapped environments with moving sounds," *IEEE Robotics and Automation Letters*, vol. 8, no. 2, pp. 928–935, 2023.
- [19] J. V. Hurtado and A. Valada, "Semantic scene segmentation for robotics," in *Deep learning for robot perception and cognition*, 2022, pp. 279–311.
- [20] L. Rustler, J. Lundell, J. K. Behrens, V. Kyrki, and M. Hoffmann, "Active Visuo-Haptic Object Shape Completion," *IEEE Robotics and Automation Letters*, vol. 7, no. 2, pp. 5254–5261, 2022.
- [21] E. Smith, R. Calandra, A. Romero, G. Gkioxari, D. Meger, J. Malik, and M. Drozdal, "3D Shape Reconstruction from Vision and Touch," in *Proc. Adv. Neural Inform. Process. Syst.*, 2020.
- [22] P. K. Murali, B. Porr, and M. Kaboli, "Touch if it's transparent! ACTOR: Active Tactile-based Category-Level Transparent Object Reconstruction," in *Proc. IEEE Int. Conf. on Intel. Rob. and Syst.*, 2023.
- [23] P. Falco, S. Lu, A. Cirillo, C. Natale, S. Pirozzi, and D. Lee, "Cross-modal visuo-tactile object recognition using robotic active exploration," in *Proc. IEEE Int. Conf. on Rob. and Auto.*, 2017.
- [24] P. Falco, S. Lu, C. Natale, S. Pirozzi, and D. Lee, "A transfer learning approach to cross-modal object recognition: from visual observation to robotic haptic exploration," *IEEE Trans. Robot.*, 2019.
- [25] M. A. Lee, Y. Zhu, P. Zachares, M. Tan, K. Srinivasan, S. Savarese, L. Fei-Fei, A. Garg, and J. Bohg, "Making Sense of Vision and Touch: Learning Multimodal Representations for Contact-Rich Tasks," *IEEE Trans. on Robotics*, vol. 36, no. 3, 2020.
- [26] S. Zhong, A. Albin, O. P. Jones, P. Maiolino, and I. Posner, "Touching a NeRF: Leveraging Neural Radiance Fields for Tactile Sensory Data Generation," in *Proc. Conf. on Rob. Learn.*, 2023, pp. 1618–1628.
- [27] B. Mildenhall, P. P. Srinivasan, M. Tancik, J. T. Barron, R. Ramamoorthi, and R. Ng, "Nerf: Representing scenes as neural radiance fields for view synthesis," *Communications of the ACM*, vol. 65, no. 1, pp. 99–106, 2021.
- [28] J.-T. Lee, D. Bollegala, and S. Luo, "Touching to See" and "Seeing to Feel": Robotic Cross-modal Sensory Data Generation for Visual-Tactile Perception," in *Proc. IEEE Int. Conf. on Rob. and Auto.*, 2019.
- [29] F. Yang, J. Zhang, and A. Owens, "Generating visual scenes from touch," in *Proc. IEEE Conf. Comput. Vis. Pattern Recog.*, 2023, pp. 22070–22080.
- [30] F. Yang, C. Feng, Z. Chen, H. Park, D. Wang, Y. Dou, Z. Zeng, X. Chen, R. Gangopadhyay, A. Owens, and A. Wong, "Binding Touch to Everything: Learning Unified Multimodal Tactile Representations," *arXiv preprint arXiv:2401.18084*, 2024.
- [31] R. Corcodel, S. Jain, and J. van Baar, "Interactive Tactile Perception for Classification of Novel Object Instances," in *Proc. IEEE Int. Conf. on Intel. Rob. and Syst.*, 2020, pp. 9861–9868.
- [32] R. Calandra, A. Owens, M. Upadhyaya, W. Yuan, J. Lin, E. H. Adelson, and S. Levine, "The feeling of success: Does touch sensing help predict grasp outcomes?" in *Proc. Conf. on Rob. Learn.*, 2017, pp. 314–323.
- [33] Q.-Y. Zhou and V. Koltun, "Dense scene reconstruction with points of interest," *ACM Trans. Graph.*, vol. 32, no. 4, 2013.
- [34] J. A. E. Andersson, J. Gillis, G. Horn, J. B. Rawlings, and M. Diehl, "CasADi – A software framework for nonlinear optimization and optimal control," *Mathematical Programming Computation*, vol. 11, no. 1, pp. 1–36, 2019.
- [35] M. Savva, A. X. Chang, and P. Hanrahan, "Semantically-Enriched 3D Models for Common-sense Knowledge," *CVPR Workshop on Functionality, Physics, Intentionality and Causality*, 2015.
- [36] C. Eppner, A. Mousavian, and D. Fox, "ACRONYM: A Large-Scale Grasp Dataset Based on Simulation," in *Proc. IEEE Int. Conf. on Rob. and Auto.*, 2021, pp. 6222–6227.
- [37] M. Sundermeyer, A. Mousavian, R. Triebel, and D. Fox, "Contact-graspnet: Efficient 6-dof grasp generation in cluttered scenes," in *Proc. IEEE Int. Conf. on Rob. and Auto.*, 2021, pp. 13438–13444.
- [38] Y. Xiang, C. Xie, A. Mousavian, and D. Fox, "Learning rgb-d feature embeddings for unseen object instance segmentation," in *Proc. Conf. on Rob. Learn.*, 2021, pp. 461–470.
- [39] C. R. Qi, L. Yi, H. Su, and L. J. Guibas, "Pointnet++: Deep hierarchical feature learning on point sets in a metric space," *Adv. in neural information processing systems*, vol. 30, 2017.